Single particle effects in precompound reactions

W. Scobel,* M. Blann, T. T. Komoto, M. Trabandt,* S. M. Grimes,† L. F. Hansen, C. Wong, and B. A. Pohl
Lawrence Livermore National Laboratory, University of California, Livermore, California 94550
(Received 26 April 1984)

Double differential cross sections have been measured with time of flight techniques at 16 angles between 3.5° and 159° (lab) for the inclusive production of neutrons from reactions of 25 MeV protons with ^{50,52,53}Cr, ^{54,56,58}Fe, ^{59}Co, ^{60}Ni, ^{63}Cu, ^{89}Y, ^{90,91,92,94}Zr, ^{92,94,95,96,97,98,100}Mo, ^{110}Pd, and ^{159}Tb and of 18 MeV protons with ^{90,91,92,94}Zr. The spectra from ^{90,91,92,94}Zr targets are compared with qualitative and quantitative predictions based on proton-particle—neutron-hole state densities generated from different sets of single particle states using the recursion method of Williams *et al.* An end point gap of nearly 4 MeV in the ^{91}Zr(p,n) spectrum may be understood quantitatively in terms of such an extreme single particle model argument. The experimental peak structure shows reasonably good agreement with the calculated results. It is shown that precompound spectra exhibit pronounced structure which is dependent upon nuclear structure effects for near closed shell nuclei, and that these effects should and do disappear rapidly with nuclear deformation, as predicted earlier by Williams *et al.*

I. INTRODUCTION

Precompound models that assume the reaction system to proceed through a series of two-body collisions have been very successful in reproducing smooth continuous spectra from a wide range of nucleon-induced reactions. Far less has been done in investigating the manner in which nuclear structure effects (as manifested by realistic single particle levels) might show up in precompound decay.

A decade has passed since Williams *et al.*[1] and Albrecht and Blann[2] predicted significant influences on precompound spectra when realistic single particle levels were considered. Little has been done to test these predictions.[3,4] In preparation of the work presented here, we have used the codes developed in Refs. 1 and 2 and modified by Grimes *et al.*[4] to select a target sequence for which significant target structure effects can be expected in the precompound (p,n) spectra. We would expect these effects to be most pronounced in regions where the single particle levels near the Fermi energy deviate strongly from an equidistant spacing description, i.e., for residual nuclei with small ground state deformation and in the region of magic numbers. It is most appropriate to study the (p,n) reaction for a sequence of shell crossing isotopes or isotones and observe the differences in structure. One target sequence for which large effects were predicted is ^{90,91,92,94}Zr. We have performed these measurements with 18 and 25 MeV projectiles, and in this work we explore the possibility of interpreting these results using shell and Nilsson model based single particle levels for the calculation of few exciton state densities.

The Zr target sequence allows us to test the influence of neutron hole structure in the residual Nb nuclei, i.e., near $N=50$, on experimental spectra. Similarly the ^{50,52,53}Cr(p,n) measurements test the region $N=28$. The ^{58}Fe, ^{59}Co, ^{60}Ni (p,n) data probe the importance of proton single particle-exciton levels near $Z=28$ on spectra. Additional targets have been measured either as controls,[4–6] (^{89}Y, ^{110}Pd, ^{159}Tb) to clean the spectra of interest from isotopic impurities (^{54}Fe, ^{56}Fe), or to seek information on the related topic of pairing effects in precompound decay ($^{92-100}$Mo). We will summarize all experimental results in Sec. II after presentation of our experimental method. However, we will only interpret the results on the Zr targets in this work; other results will be interpreted in later works.

Section III is devoted to a discussion of the qualitative details as to how the nuclear structure of the targets should influence details of the experimental (p,n) precompound spectra, and as to the calculation of few quasiparticle densities and the options available in such calculations. We will show structure effects expected for near-closed-shell nuclei, and illustrate how these effects are predicted to disappear rapidly with target deformation. In Sec. IV we will compare experimental results of this work with particular sets of theoretical predictions based on such calculations (Refs. 1, 2, and 4). Our conclusions are given in Sec. V.

II. EXPERIMENTAL METHODS AND RESULTS

A. Time-of-flight facility

The experiment was performed with the proton beam of the Lawrence Livermore National Laboratory Cyclograaff accelerator using beam energies of 25.0±0.08 MeV and 18.0±0.08 MeV.[7,8] The 24.93 MHz repetition rate of the AVF cyclotron was scaled down by a factor of 10 with two external sweepers to allow for neutron time-of-flight (TOF) spectroscopy with 10.75 m flight paths without ambiguities due to overlapping bursts in the neutron energy range under consideration ($E_n \geq 3.5$ MeV). The geometry of the TOF area is shown in Fig. 1.

Neutron TOF spectroscopy was performed simultaneously at 16 angles between 3.5° and 159°. The detectors

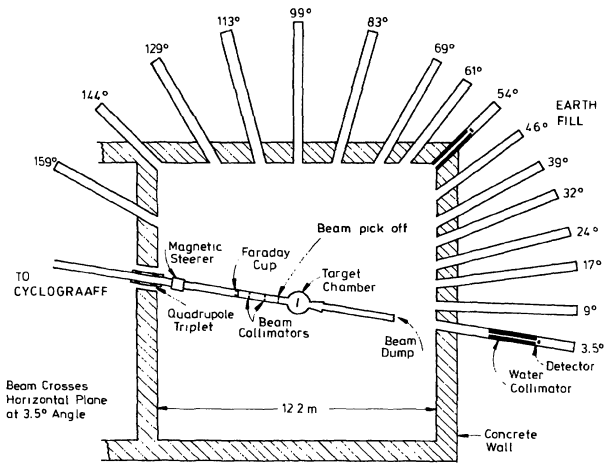

FIG. 1. Schematic diagram of the time of flight target and detector geometry. A removable Faraday cup position is shown. Target current readings are taken from the beam dump, which is a shielded Faraday cup.

were 11.4 cm $\varnothing \times 5.1$ cm NE213 scintillators behind water collimators of 2 m length, surrounded by a shield of earth and concrete. The efficiencies of the liquid scintillators were calculated with the code EFFIC. The results have been reported[8] to deviate from those of the code DETEFF by at most $\pm 7\%$; in addition the absolute differential cross sections of the ^{2}H(d,n)^{3}He measured at $E_d = 10$ MeV and analyzed with these efficiencies showed good agreement with existing data. The Livermore multidetector setup is described in detail elsewhere;[9] the subsequent description is therefore restricted to features specific to our measurements.

B. Experimental setup

The proton beam was focused through insulated, adjustable collimators and the 5–20 μg/cm^2 carbon foil of the time pickoff unit[10] onto the target which was mounted 90 cm behind the beam pickoff (in a thin walled scattering chamber); after passing through the target the beam was dumped into a shielded Faraday cup approximately 430 cm behind the target. The integrated Faraday cup current was recorded for absolute cross section determination.

The targets were self-supporting, isotopically pure or enriched metallic foils of 2.38 cm diam and thicknesses ranging from 1.9 to 5.5 mg/cm^2 (see Table I). The effective thickness in the region of the beam spot of about 6 mm diam was deduced[11] from the measured energy degradation of ^{241}Am α particles ($E_\alpha = 5.48$ MeV); results are given in Table I. Additional properties of the targets investigated are summarized in Table II.[12,13]

Conventional electronics were used with the individual neutron TOF detectors. A linear bias was set individually for each detector at the pulse height of two times the half-value of the Compton edge from 1.275 MeV γ radiation (^{22}Na), which is equivalent to a minimum proton recoil energy $E_n^{min} = 5.4$ MeV. For the $E_p = 18$ MeV runs this threshold was lowered by a factor of 2, yielding $E_n^{min} = 3.5$ MeV. The γ radiation background was effectively suppressed by the pulse shape discrimination applied. Some typical TOF spectra resulting from runs at 25 MeV with the ^{90}Zr target are shown in the left column of Fig. 2 for the laboratory angles $\theta_{lab} = 3.5°$, 32.3°, and 128.7°, respectively. The energy scale is deduced from the position of the target γ peak and the time calibration of the system.

C. Background corrections

The influence of background neutrons on continuous neutron energy spectra taken with the Livermore TOF facility has been discussed in detail elsewhere.[5] There, a comparison of three different treatments of background corrections was performed for (p,xn) reactions, namely (i) extrapolation from the unphysical TOF region ($t = E_n > 25$ MeV) under the assumption of random distribution in time, i.e., no correlation, (ii) background runs with an empty target frame, and (iii) background runs with shadow bars being inserted in the TOF path halfway between target and water collimators in front of the detectors. The results[5] may be summarized as follows.

For a carefully focused beam and for all angles but the two extreme ones, procedure (i) accounts for most of the background. This background is approximately a 10% correction in the region $E_n = 3$–15 MeV for reactions of 26 MeV protons with ^{65}Cu and ^{89}Y. Inspection of the background spectra (ii) obtained with the empty target frame indicates an additional background component that is correlated in time with the beam; it has a smooth structure in the physical region and is not accounted for by the extrapolation (i). The background runs (iii) with shadow bar include the contribution of room-scattered neutrons produced in the target. The differences to correction (ii) are small with the exception of the 3.5° position, where small angle scattering of reaction neutrons along the (flared) beam pipe leading to the beam dump enhances the yield.

In the present experiment, background runs with an empty frame (ii) were performed sufficiently often, normalized to the target runs and subtracted. The remaining uncorrelated background was taken care of as under (i). This treatment may still be insufficient, if the beam has no long term stability. Analysis of the geometry, in particular of the pickoff and of the collimation near to the reaction chamber, reveals that only the detectors at 3.5°, 9.2°, 16.7°, and 159° may be influenced.

Some typical spectra are presented in Fig. 2. The TOF spectra show a constant background level in the unphysical region ($E_n > E_{n,max}$) which has the same height for both target and empty frame runs. Therefore the data treatments (i) and (ii) yield the same result in this region. This holds for the unphysical region, too, in case of the angles 32.3° and 128.7°, where the background represents a 10% correction; for the 3.5° run, the background is considerably higher and cannot be accounted for by procedure (i). Hence, procedure (ii) is used for background subtraction. However, the spectra taken at 9.2° already show greater similarity to those at 32.3° than with the 3.5° data. At all angles, the background spectra are rather

TABLE I. Target foils and composition.

Target	Target thickness (mg/cm^2)	Isotopic constituents A(%)	Charge accumulated (mCi)
$^{50}_{24}Cr$[a]	3.3	50(95.9),52(3.8)	1.34
$^{52}_{24}Cr$[a]	2.3	52(99.9)	1.50
$^{53}_{24}Cr$	2.3	53(96.4),52(3.4),54(0.2)	1.50
$^{54}_{26}Fe$	5.3	54(96.8),56(3.0)	1.50
$^{56}_{26}Fe$	5.3	56(99.9)	1.20
$^{58}_{26}Fe$	5.4	58(76.66),56(23)	1.31
$^{59}_{27}Co$	4.4	59(100)	1.50
$^{60}_{28}Ni$	4.1	60(99.8)	1.50
$^{63}_{29}Cu$	4.1	63(99.9)	1.30
$^{89}_{39}Y$	3.4	89(100)	1.50
$^{90}_{40}Zr$	6.2	90(97.65),91(0.96),92(0.71),94(0.55)	1.50;0.9[b]
$^{91}_{40}Zr$	5.7	91(88.5),90(6.51),92(3.21),94(1.61)	1.00[a];0.9[b]
$^{92}_{40}Zr$	5.3	92(95.13),90(2.54),91(1.04),94(1.11)	0.94;1.0[b]
$^{94}_{40}Zr$	5.4	94(96.49),90(1.91),91(0.51),92(0.85)	0.75;0.5[b]
$^{92}_{42}Mo$[a]	4.9	92(98.3),94(0.5),95(0.4),96(0.3), 97(0.1),98(0.3),100(0.3)	1.5
$^{94}_{42}Mo$	2.6	94(93.9),92(0.9),95(2.9),96(1.0), 97(0.4),98(0.8)	1.8
$^{95}_{42}Mo$	5.3	95(96.8),92(0.3),94(0.6),96(1.5), 97(0.4),98(0.5)	1.4
$^{96}_{42}Mo$	2.6	96(96.8),92(0.2)94(0.2),95(0.9), 97(1.0),98(0.8),100(0.1)	1.9
$^{95}_{42}Mo$	2.1	97(92.8),92(0.3)94(0.2),95(0.7), 96(1.7),98(4.0),100(0.4)	1.55
$^{98}_{42}Mo$	2.1	98(97.0),92(0.3),94(0.2),95(0.5), 96(0.6),97(0.8),100(0.6)	2.0
$^{100}_{42}Mo$	2.6	100(95.9),92(0.9),94(0.3),95(0.4), 96(0.6),97(0.4),98(1.5)	1.50
$^{110}_{46}Pd$	5.4	110(95.2),108(3.7),106(0.1)	1.0
$^{159}_{65}Tb$	4.1	159(100)	1.0

[a]The (p,n) measurement of this target has been repeated for checking.
[b]Accumulated charges refer to $E_p = 18$ MeV runs.

TABLE II. Reaction data. Excitation energies E^* (IAS) of the isobaric analogs are from Ref. 12 or, if in parentheses, calculated from Ref. 13. Maximum kinetic energies $E_{n,max}$ of the neutrons refer to the c.m. system and are given in parentheses for 18 MeV projectiles; "is" denotes spin isomers.

Reaction	I^π Target	I^π Product	Q(p,n)	E^* (IAS) (MeV)	$E_{n,max}$
$^{50}_{24}Cr(p,n)^{50}_{25}Mn$	0^+	0^+	−8.41	0.0(g.s.)	15.77
$^{52}Cr(p,n)^{52}Mn$	0^+	6^+	−5.49	2.93	18.67
$^{53}Cr(p,n)^{53}Mn$	$\frac{3}{2}^-$	$\frac{7}{2}^-$	−1.38	6.97	22.72
$^{54}_{26}Fe(p,n)^{54}_{27}Co$	0^+	0^+	−9.03	0.0(g.s.)	15.23
$^{56}Fe(p,n)^{56}Co$	0^+	4^+	−5.35	3.56	18.88
$^{58}Fe(p,n)^{58}Co$	0^+	2^+	−3.09	5.75	21.11
$^{59}_{27}Co(p,n)^{59}_{28}Ni$	$\frac{7}{2}^-$	$\frac{3}{2}^-$	−1.86	7.34	22.34
$^{60}_{28}Ni(p,n)^{60}_{29}Cu$	0^+	2^+	−6.91	2.55	17.38
$^{63}_{29}Cu(p,n)^{63}_{30}Zn$	$\frac{3}{2}^-$	$\frac{3}{2}^-$	−4.15	5.50	20.13
$^{89}_{39}Y(p,n)^{89}_{40}Zr$	$\frac{1}{2}^-$	$\frac{9}{2}^-$	−3.62	8.09	20.86
$^{90}_{40}Zr(p,n)^{90}_{41}Nb$	0^+	$8^+;4^-$(is)	−6.89	5.11	17.63(10.79)
$^{91}Zr(p,n)^{91}Nb$	$\frac{5}{2}^+$	$\frac{9}{2}^+;\frac{1}{2}^-$(is)	−2.04	9.82	22.44(15.59)
$^{92}Zr(p,n)^{92}Nb$	0^+	$7^+;2^+$(is)	−2.79	9.03	21.70(14.85)
$^{94}Zr(p,n)^{94}Nb$	0^+	$6^+;3^+$(is)	−1.68	(10.0)	22.81(15.96)
$^{92}_{42}Mo(p,n)^{92}_{43}Tc$	0^+	(8^+)	−8.65	3.81	15.90
$^{94}Mo(p,n)^{94}Tc$	0^+	$7^+;(2^+,$is)	−5.04	(7.3)	19.49
$^{95}Mo(p,n)^{95}Tc$	$\frac{5}{2}^+$	$\frac{9}{2}^+;\frac{1}{2}^-$(is)	−2.48	9.82	22.02
$^{96}Mo(p,n)^{96}Tc$	0^+	$7^+;4^+$(is)	−3.76	8.44	20.77
$^{97}Mo(p,n)^{97}Tc$	$\frac{5}{2}^+$	$\frac{9}{2}^+;\frac{1}{2}^-$(is)	−1.10	11.02	23.40
$^{98}Mo(p,n)^{98}Tc$	0^+	$(6)^+$	−2.46	9.74	22.05
$^{100}Mo(p,n)^{100}Tc$	0^+	1^+	−0.95	(10.9)	23.56
$^{110}_{46}Pd(p,n)^{110}_{47}Ag$	0^+	$1^+;6^+$(is)	−1.67	(11.2)	22.90
$^{159}_{65}Tb(p,n)^{159}_{66}Dy$	$\frac{3}{2}^-$	$\frac{3}{2}^-$	−1.15	15.18	23.54

smooth and no individual structures are observed. Therefore the background cannot be responsible for structure persisting in the spectra after background subtraction.

D. Measurements and raw data reduction

The measurements were performed with proton beam intensities of the order of 50 nA; the integrated charges given in Table I were accumulated in runs which were typically 8 h duration. On the average, three additional hours were spent on background runs of type (ii). The burst widths measured over a short time interval had about 1.0 ns FWHM, yielding a long term system time resolution of ~ 1.5 ns. This corresponds to an energy resolution $WE_n \approx 125$ keV (350 keV) at $E_n = 10$ MeV (20 MeV).

After background subtraction the TOF spectra were converted into energy spectra in the center of mass frame with the detector efficiencies calculated as described in Sec. II A and under the assumption of single nucleon emission. The uncertainties ΔE_n for neutrons actually stemming from second chance emission are at most equal to the recoil correction for the highest possible nucleon energy (~ 10 MeV) allowing for secondary emission of neutrons with energies above the detection threshold, i.e., $|\pm\Delta E_n| \leq 100$–200 keV for the target masses under consideration. The rare events of neutrons following α emission can be neglected.

These energy widths suggest use of energy bin sizes of at least 200 keV. Spectra obtained at different angles are shown for all systems under investigation in Ref. 14. A complete listing of these data averaged over 200 keV bins including statistical uncertainties is also given in Ref. 14. A representative set of results for ^{90}Zr is shown in Fig. 3.

All targets show the isobaric analog ground state transitions (IAS), whose positions and widths confirm the correct and consistent transformation of the time into neutron center-of-mass energy spectra as well as the energy resolution stated above. For ^{50}Cr and ^{54}Fe the analog state[12] is identical with the ground state of the residual nucleus.

All data of this work refer to isotopically pure targets. The correction for isotopic impurities was possible, because for the elements Mo, Zr, Cr, and Fe we have measured the (p,n) reaction for all relevant isotopes (see Table I) such that the c.m. energy spectra could be consistently unfolded. The remaining targets were either highly enriched or isotopically pure. This final set of data will be used for comparisons with calculated results and may be found in tabular form in Ref. 14.

The main systematic uncertainties arise from the neutron detector efficiency (7%), the effective target thickness due to inhomogeneities and uncertainties of the energy-range tables (5%), and incomplete beam current integration (3%) and sum up to 9%. To this number the

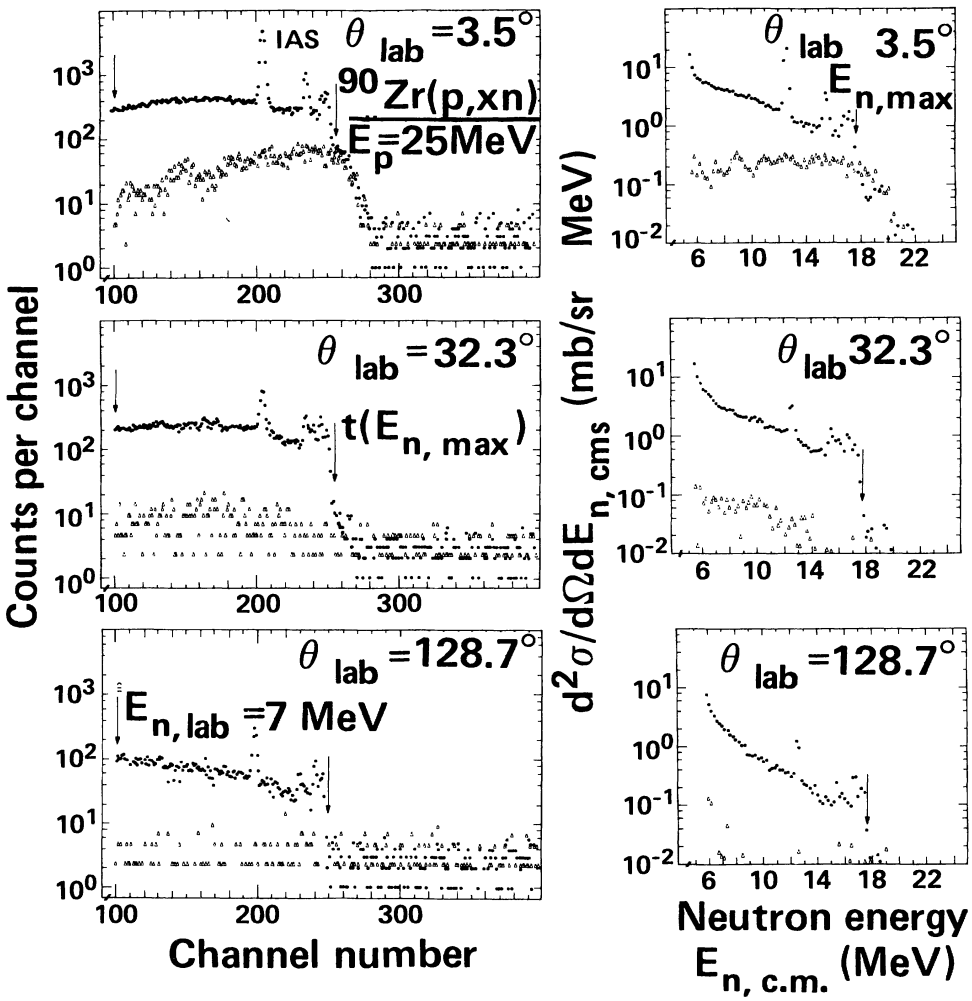

FIG. 2. Experimental ^{90}Zr(p,xn) spectra and associated background spectra at 3.5°, 32.3° and 128.7°. The figure is discussed in the text. The most prominent peak is the IAS ground state; the downward arrow at high energy shows the end point energy. The downward arrow at low energy shows the cut off energy of the measurement.

uncertainty in background subtraction ($\leq 5\%$, but higher at 3.5°, cf. Sec. II C) and the statistical uncertainties that depend on target, angle, and neutron energy have to be added. The overall uncertainties therefore range from 11% for angle integrated cross sections, and for double differential cross sections in the evaporation region and for the forward hemisphere; at higher neutron energies and for backward angles the estimates for the double differential cross sections approach 30%, and may be even higher for the low neutron yield reactions (e.g., p+^{50}Cr,^{54}Fe,^{92}Mo). The measured spectra for ^{50}Cr, ^{52}Cr, ^{91}Zr, and ^{92}Mo have been reproduced in independently repeated runs within the statistical uncertainties claimed.

III. SINGLE PARTICLE BASED PARTIAL STATE DENSITIES

A. Qualitative expectations of spectral effects

In this section we adopt the picture of a nucleon induced reaction as proceeding through a series of nucleon-nucleon interactions towards an equilibrated system. We may then discuss the manner in which (p,n) emission spectra would be expected to reflect single particle structure to the degree that single particle energies may be described by pure shell model energies without gross perturbation due to residual interactions. We will concentrate on the one-particle—one-hole residual configuration of the precompound exciton hierarchy, as this will be by far the most important contributor to the experimental spectra at the emission energies and for the residual excitations of interest.

For a (p,n) reaction, the first precompound hierarchy ($n_0=3$) is described as two-particle—one-hole; if a neutron is to be emitted, the three exciton configuration must be $(p)(n)(n)^{-1}$ in nature. The residual nucleus will therefore remain in a $(p)(n)^{-1}$ state. The energy spectrum of the emitted neutron may be expected to be influenced by the spectral distribution of $(p)(n)^{-1}$ states accessible following a two-body interaction of the projectile proton with target neutrons.

For reactions on Zr isotopes, qualitative insights into

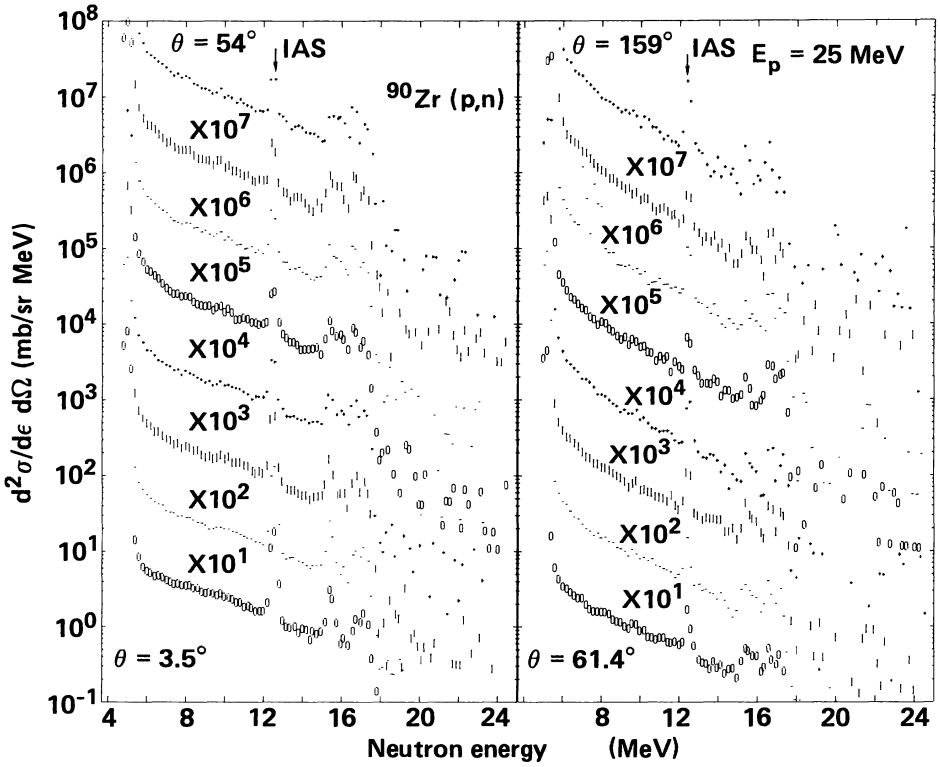

FIG. 3. Doubly differential spectra for the ^{90}Zr(p,xn) reaction for 25 MeV incident proton energy. These are data, before isotopic composition corrections. They are typical of the data measured in the course of this work. The vertical lines represent the end point (ground state). The angles represented begin at 3.5° in the lower left of the figure, increasing to 54° at the top left (see Fig. 1 for intermediate angles). Angles begin at 61.4° in the lower right, increasing to 159° in the upper right. Energies are in the center-of-mass system.

shell structure effects on single particle levels may be gained by reference to Fig. 4, where calculated[15] shell model levels are shown for target neutrons. For ^{90}Zr the ground state may be populated when the incident proton interacts with any of the ten neutrons filling the $g_{9/2}$ level. If the neutron is emitted in a ground state transition (i.e., maximum kinetic energy), the proton may enter any of the ten degenerate $g_{9/2}$ levels, all of which are vacant in the target nucleus. Ground state transitions may therefore be made in many different ways (due to the large number of degenerate orbitals) and the precompound (p,n) transition to the ground state would be expected to be strong. In this context, we emphasize that we consider knockon contributions usually referred to as "direct" to be included in the precompound mechanism.[16]

The situation changes drastically by adding a single neutron to the target, i.e., using a ^{91}Zr target. Of course, the proton following the two-body interaction has the same multiplicity of low lying orbitals available as for the ^{90}Zr target; however, the ground state may *only* be populated if the proton interacts with the lone $d_{5/2}$ neutron. If the proton interacts with any other neutron, then the emitted neutrons will have less than the ground state energy by at least the $d_{5/2}$-$g_{9/2}$ energy difference (about 4 MeV in Fig. 4). We therefore would expect a small discrete ground state transition, a gap of around 4 MeV, and then a spectrum looking very much like the ^{90}Zr(p,n) spectrum displaced by the $d_{5/2}$-$g_{9/2}$ level spacing. For the case of a ^{92}Zr target, we expect a situation similar to that for ^{91}Zr, but with a larger ground state transition cross section corresponding to two $d_{5/2}$ neutrons which may participate in a ground state transition. Going to

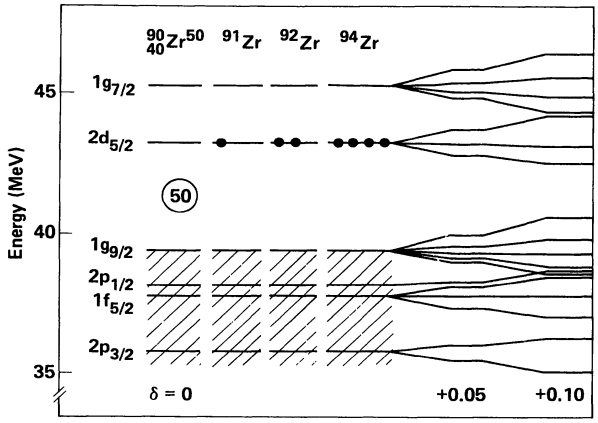

FIG. 4. Schematic diagram showing single particle levels for Zr isotopes using the Seeger-Howard (Ref. 15) single particle spacings. Deformation parameters of δ=0, +0.05, and +0.1 are shown. Occupation of the $2d_{5/2}$ levels by neutrons is indicated by solid circles.

^{94}Zr with four neutrons in the $d_{5/2}$ level, the argument may be extended.

However, additional factors come into play when considering ^{94}Zr and probably ^{90,92}Zr. As the residual nucleus gets further from closed shell configurations, the $d_{5/2}$ and $g_{9/2}$ single particle strengths will spread leading to configuration mixing. In addition, the nuclei may have nonspherical ground and excited states; the Nilsson model then predicts a decrease of the gap and of the single particle level bunching (Fig. 4), resulting in a reduced Rosenzweig[17] effect. These effects will tend to smooth the consequences of the extreme shell model arguments we have presented thus far. This smoothing is indeed seen in the experimental data.

The angle integrated ^{90,91,92,94}Zr(p,n) spectra measured for $E_p=18$ and 25 MeV are shown in Fig. 5. The qualitative differences described above are observed very clearly in the experimental results. In Fig. 5 we also show spectra calculated with the geometry dependent hybrid model using the usual equidistant spacing model for calculating exciton state densities.[18–20] While the calculation does extremely well at a lower neutron energy (higher residual excitations), gross discrepancies are noted for transitions to low excitations. These may be understood qualitatively by reference to Fig. 4 and the preceding discussion. We wish to explore how quantitatively these effects may be understood in the remainder of this work. In the following subsections we describe calculations of few-quasiparticle densities which may be compared on a more quantitative basis with the (p,n) spectra measured in this work.

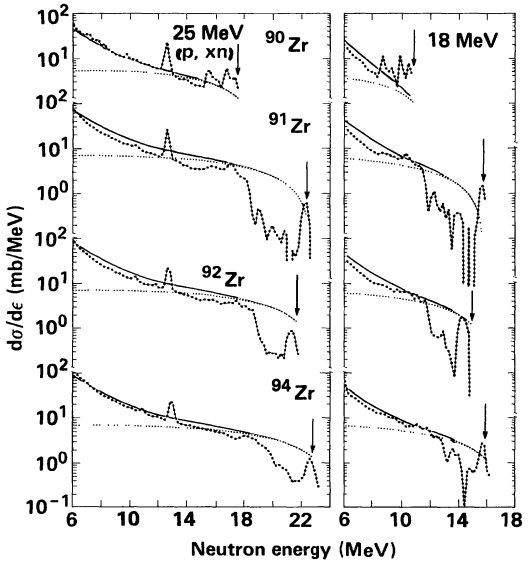

FIG. 5. Calculated and experimental (p,xn) spectra for proton energies of 18 and 25 MeV on targets of ^{90,91,92,94}Zr. Solid points represent the experimental angle integrated data corrected for background and for isotopic impurities. The solid curves are results of the geometry dependent hybrid model plus evaporation model calculations. The dotted curves are the contribution of the first ($n_0=3$) exciton number to the total calculated neutron spectra. Arrows represent end point energies.

B. Generation of few quasiparticle state densities

The few exciton state densities $\omega(Q,N)$ for N similar fermions above the Fermi energy and a total excitation energy Q were calculated from a set of single particle energies $\epsilon_i=E_i-E_F$ with respect to the target Fermi energy[2] E_F by means of the recursion relation[1]

$$\omega_i(Q,N)=\omega_{i-1}(Q,N)+\omega_{i-1}(Q-\epsilon_i,N-1)\ . \tag{1}$$

The recursion index i refers to the ith single particle energy. The state density $\omega(U,N_H)$ for N_H holes that share the excitation energy U can be calculated similarly. The recursion converges rapidly. These results are then folded to give the particle-hole state density $\omega(Q,N,N_H)$:

$$\omega(Q,N,N_H)=\sum_{U=0}^{Q}\omega(U,N)\omega(Q-U,N_H)\ . \tag{2}$$

If both kinds of nucleons share the excitation energy E^*, an equivalent calculation starting from the corresponding set of single particle levels gives $\tilde{\omega}(Q,Z,Z_H)$. Folding of both results then yields the final partial state density

$$\omega(E^*,N,N_H,Z,Z_H)=\sum_{Q=0}^{E^*}\tilde{\omega}(Q,Z,Z_H)\omega(E^*-Q,N,N_H)\ . \tag{3}$$

It should be noted that these densities are defined by energy only, with no information maintained on the angular momentum distribution; we will discuss the significance of this point in greater detail further on in this work.

C. Single particle levels

The type of investigation we present here is relatively new; therefore there are still uncertainties and ambiguities in the choice of the parameters entering into the single particle level calculation and their combination to give "realistic" partial state densities. We will describe the options of the codes used and show in some examples how the results vary with the input parameters. A "best" set of parameters will be deduced by comparison with experimental data rather than on pure theoretical reasoning.

We consider three choices of single particle levels that are generated internally in the codes used, namely those due to the Nilsson model with the parametrization of Nilsson,[21] Seeger and Howard[15] or Seeger and Perisho.[22] Potential shapes are restricted to quadrupole deformations, where the input parameter δ is related to the Nilsson parameter η

$$\eta=\frac{\delta}{\kappa}(1-\tfrac{4}{3}\delta^2-\tfrac{16}{27}\delta^3)^{-1/6} \tag{4}$$

and κ is the nucleon and shell dependent strength of the spin orbit term.

Not only shell effects, but also pairing will cause energy shifts of total and partial state densities.[4] Pairing energies may be treated either by a constant shift depending on the odd-even type of the residual system,[3,19] or by replacing the single particle energies $\epsilon_i=E_i-E_F$ by quasiparticle energies $\epsilon_i'=(\epsilon_i^2+\Delta^2)^{1/2}$. For the ground state, the gap

parameter Δ may be calculated from the gap equation

$$\frac{2}{G}=\sum_i \frac{1}{\epsilon_i'} \tag{5}$$

of the Bardeen, Cooper, and Schrieffer (BCS) formalism,[23] and E_F is fixed by the requirement (for the example of N neutrons)

$$N=\sum_i \left[1-\frac{E_i-E_F}{[(E_i-E_F)^2+\Delta^2]^{1/2}}\right]. \tag{6}$$

The summations extend over the doubly degenerate orbitals and G is the constant pairing strength. The formalism assumes equal diagonal and off-diagonal matrix elements between each $J=0$ coupled pair.

In view of these approximations, it seems justified to add another one that considerably simplifies the calculation: We assume that Δ does not change with the excitation energy E^*, such that the ground state values can be used throughout.

Finally the state densities obtained from Eq. (2) are smoothed with a Gaussian distribution characterized by its standard deviation σ before they are folded according to Eq. (3). This treatment prepares the calculation for comparison with the experimental data which are broadened by the experimental resolution, and, what is more important, it may roughly account for the spreading of the single particle strengths due to residual interactions.

There are a number of reasons that the theoretically predicted structure should deviate from results in nature both in peak width and position. We may summarize several of these as follows:

(1) The calculation considers only the energies of the single particle levels; however, each residual interaction and coupling of the angular momenta of unpaired particles should yield different level energies rather than the degenerate results assumed in our codes.

(2) The targets used, due to being closed shell or near-closed shell in nature, involve single particle orbitals which may have very large ranges of angular momenta to which they may couple. The reaction kinematics may strongly select against population of some of these levels due to the kinematically allowed orbital angular momentum transfers. These restrictions are not considered (as yet) in our codes for generating few quasiparticle densities.

(3) Positions calculated for excited single particle levels will be even more sensitive to details of the shape of the assumed potential well than for lower lying orbitals (see Fig. 4).

(4) As particle orbitals become unbound, the shell model levels become questionable in meaning; the centrifugal barrier, and for protons the Coulomb barrier, may mitigate this point for a few MeV. For ^{90,91,92,94}Nb, the proton binding energies are 5.2, 5.8, 6.0, and 6.8 MeV, respectively.

(5) As the single particle energies increase the lifetime decreases, and the natural width due to the Heisenberg principle increases. Similarly, the spreading width will change. We might therefore expect that the constant averaging width of our calculation might better be replaced by an energy dependent function.

(6) The excited state nuclei, which may have high ($\approx 9\hbar$) angular momenta, may have deformations larger than the ground state target nuclei.

In spite of these many reasons to expect failure, we nonetheless wish to make the comparisons under discussion, but with a realistic outlook as to what constitutes success.

D. Parameter sensitivities

In Fig. 6 we illustrate for ^{92}Nb the $(p)(n)^{-1}$ state densities using each of the three[15,21,22] sets of single particle states for a spherical potential. The BCS approach has been chosen for the treatment of the residual (pairing) interaction. The ground state pairing energies Δ_n and Δ_p were those of Gilbert and Cameron[24] that have proven to be a good approximation of the values obtained from an exact BCS calculation of the total level densities in the mass range $A\approx 60$.[25] A smoothing width $\sigma=1$ MeV was applied. A reasonably large variation of structure positions may be seen to result from the different input choices.

The influence of σ may be seen in Fig. 7, where the results for the values 1.0, 1.5, 2.0, and 3.0 MeV are shown for the Seeger-Perisho single particle set, again for the nucleus ^{92}Nb. We have adopted the 1.5 MeV smoothing width for further comparisons between calculated and experimental results. The choice was made on a purely arbitrary basis because it gives peak widths similar to experimental results. There are reasons as to why the width σ should actually increase with increasing excitation as was mentioned in Sec. III C.

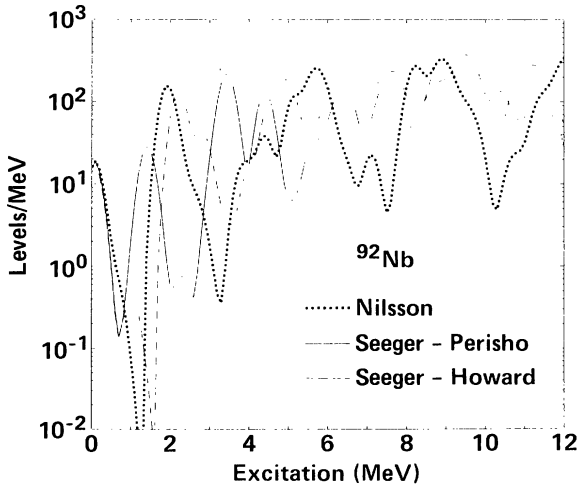

FIG. 6. Two quasiparticle densities resulting from single particle levels due to Nilsson, Seeger-Howard, and Seeger-Perisho. All calculations are for $(1p)(1n)^{-1}$ densities for spherical nuclei with $\sigma=1.0$ MeV.

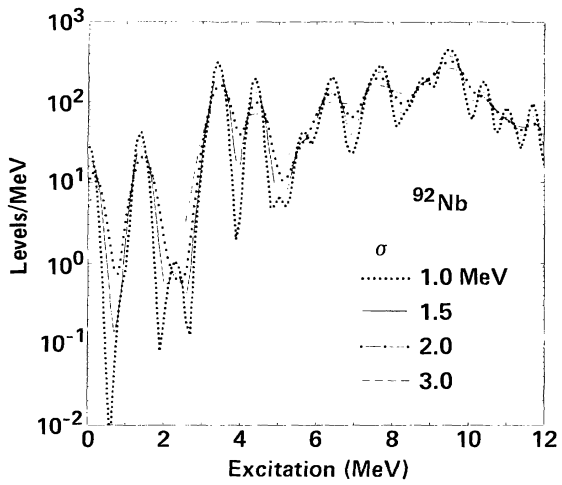

FIG. 7. Two quasiparticle densities generated with single particle levels due to Seeger-Perisho as a function of the averaging width σ. All results are for spherical nuclei ($\delta=0$).

E. Deformation

Isotopes of Zr would be expected to be spherical or nearly spherical in their ground states. However, the residual nuclides we are interested in are not $Z=40$, but $Z=41$, with mostly odd neutron numbers. We are interested not in ground states, but in excited states for which spins up to $9\hbar$ could easily result. Under these conditions deformations quite different than those appropriate to ground state values in Zr isotopes may be expected.

The Lund group has made extensive investigations of potential energy surfaces for a variety of isotopes in their ground states, but with different values of the angular momentum.[26] Their results for neutron numbers of 48–54 and for $Z=40$ and 42, for angular momenta of zero and $10\hbar$, are helpful guides for this work. Certainly the excited state deformations may reasonably be expected to be at least as large as the ground state values. We therefore summarize some of the Lund group results presented by Åberg.[26]

For angular momentum of zero, ground states had $\delta \leq 0.023$ for $N=48$–54 for $Z=40$ and 42. For $N=48$, nuclei were soft (meaning a change in potential energy with deformation less than 1 MeV) for $\delta \approx 0.1$; for $N=50$ for $\delta \approx 0.06$; for $N=52$ for $\delta \approx 0.1$, and for $N=54$ for $\delta \approx 0.2$. These numbers refer to calculations including pairing interactions.

For angular momentum $10\hbar$ all nuclei were predicted to have static ground state deformations. For $N=48$ and 50, $\delta=0.053$; for $N=52$, $\delta=0.14$; and for $N=54$, $\delta=0.17$. The rotating nuclei also are predicted to be soft against larger or smaller deformations than those we have listed, although the range is less than for the nonrotating nuclei.

The numbers given above are intended to show reasonable ranges of deformation parameters we might use in our partial state density calculations. We will accordingly present comparisons influenced by the potential surfaces of Åberg[26] as summarized herein.

IV. COMPARISONS OF CALCULATED TWO QUASIPARTICLE DENSITIES WITH EXPERIMENTAL SPECTRA

A. Relationship between spectra and densities

The hybrid model[27] for precompound decay may be written as

$$\frac{d\sigma_\nu}{d\epsilon}(\epsilon)=\sigma_R \sum_{n=n_0}^{\bar{n}} {}_nX_\nu \left[\frac{\rho_{n-1}(U)}{\rho_n(E^*)}\right]\left\{\frac{k\sigma(\epsilon)\epsilon}{[k\sigma(\epsilon)\epsilon+\lambda_+]}\right\}D_n \ . \tag{7}$$

In Eq. (7) $d\sigma(\epsilon)/d\epsilon$ is the differential spectrum for observation of particle ν (neutron or proton) with channel energy ϵ; σ_R is the reaction cross section. The summation is over exciton number of the multiple scattering hierarchy beginning with $n_0=3$ for nucleon induced reactions, increasing by $\Delta n=2$; ${}_nX_\nu$ is the number of particle excitons of type ν. The numerator in the first set of brackets is the density of final states, which for the first term would be one-particle–one-hole (1p-1h) in nature for nucleon induced reactions. While continuous exciton density functions of the Ericson-Williams–type[1,20] have generally been used for this function, the point of this work and earlier works[1,2] is that instead of $\rho_{n-1}(U)$ a state density $\omega(U,N,N_H,Z,Z_H)$ based on realistic single particle levels might be more appropriate for near-closed-shell nuclei.

The set of curly brackets in Eq. (7) exhibits the ratio of emission rate into the continuum given by the product of a constant k with an inverse cross section $\sigma(\epsilon)$ and the channel energy ϵ. The inverse cross section for neutrons increases as channel energy decreases. The product $k\sigma\epsilon$ in the numerator in Eq. (7) is therefore fairly constant over the high channel energy region of the emission spectrum when compared with $\rho_{n-1}(U)$ over the corresponding residual excitation energies $U=E^*-B_\nu-\epsilon$, where B_ν is the binding energy of the particle of the type ν.

We consider only the leading term in the precompound spectra (1p-1h residual configuration) since this term dominates at the lowest excitations where our extreme single particle model assumptions have the best chance of being valid. In Fig. 5 we have indicated the calculated contribution of the $n_0=3$ precompound decay term separately from the total calculated spectrum, as a guide to the energy region dominated by the $n_0=3$ term of Eq. (7) (actually in the geometry dependent version[18]) as calculated with the ALICE/LIVERMORE 82 code,[28] using a version which was modified to use a variable energy mesh size.

We can therefore approximate the dependence of $d\sigma/d\epsilon$ in first order by

$$\frac{d\sigma}{dU} \sim \rho_{n-1}(U) \tag{8}$$

and perform on this basis a comparison of the experimental values of $d\sigma/dU$ with the calculated one-(proton)-particle–one-(neutron)-hole state densities $\omega(U,0,1,1,0)$ to see the extent to which our calculated extreme single particle model state densities agree with experimental observation.

B. Analyses of Zr(p,n) spectra

Comparisons between experimental (p,n) spectra and $(1p)(1n)^{-1}$ two quasiparticle densities for Nb isotopes are shown in Figs. 8—10. Calculations were made with single particle levels due to Seeger-Howard or Seeger-Perisho as indicated. An energy averaging width of 1.5 MeV was applied to all results, and neutron and proton pairing energies based on results of Gilbert and Cameron were used.[24] The latter were used in the BCS approximation. Ranges of deformation were used for each isotope based on calculations of Ref. 26, and as indicated in Figs. 8—10. In Figs. 8—10 we have illustrated the effects on calculated two quasiparticle densities resulting from choice of single particle levels (Ref. 15 or 22), deformation and sign of deformation. We have plotted three sets of experimental results in Figs. 8—10. The angle integrated spectra at 18 and 25 MeV are shown, and the 9.2° double-differential spectra for 25 MeV incident proton energy have been shown.

There are two reasons we wish to compare spectra at a single (forward) angle in addition to the angle integrated results. The more significant reason is that our calculation does not consider the important restrictions on angular momentum coupling on experimental spectra. Comparisons of differences in prominent peak structure between the 9.2° measurement and angle integrated results illustrate this point. We should therefore pay greater attention to the location of calculated and experimental peak structures than to their absolute magnitudes until such time as angular momentum coupling is treated in the calculations. We emphasize that the peak positions do not change with angle, but that the relative intensities do. (We remind the reader that spectra at all angles are

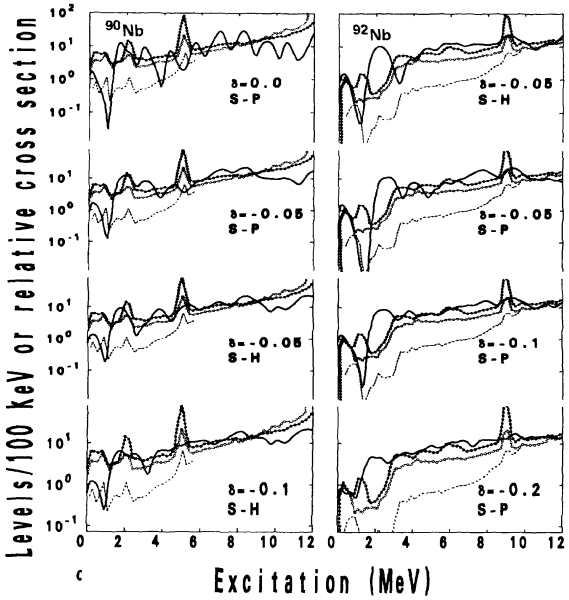

FIG. 8. Experimental and calculated results for ^{90,92}Nb nuclei. The heavy solid curves represent the $(1p)(1n)^{-1}$ two quasiparticle densities calculated using Seeger-Howard (SH) or Seeger-Perisho (SP) single particle levels with deformation parameters δ as indicated. Densities are plotted as levels/MeV; experimental spectra are plotted on a relative cross section basis; only peak shapes and positions should be compared between experimental and calculated results. Experimental spectra are plotted versus residual excitation energy, as are the two quasiparticle densities. Open circles joined by lines are angle integrated spectra from 25 MeV proton bombardment. Solid circles joined by lines are spectra measured at 9.3° (25 MeV incident proton energy). Plus signs (+) joined by lines are angle integrated spectra resulting from 18 MeV data which in this figure and in following figures have been displaced as convenient for figure clarity. Absolute values may be seen in Fig. 5.

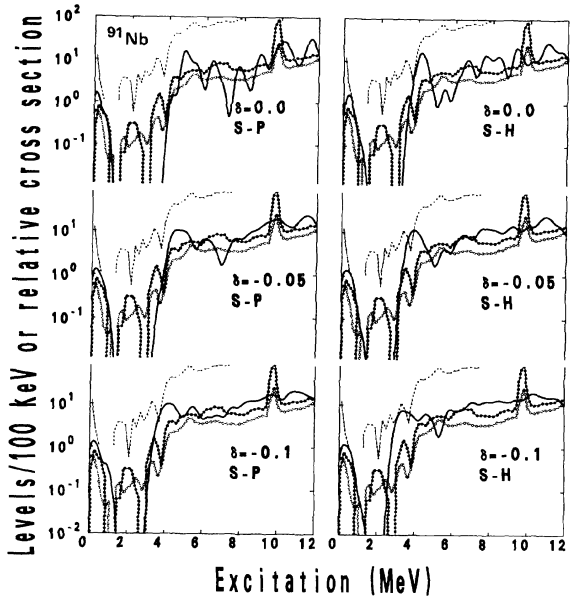

FIG. 9. As in Fig. 8 for ^{91}Nb.

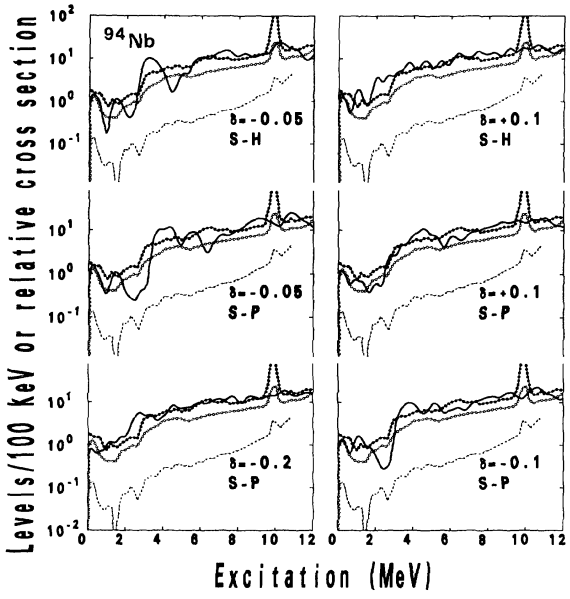

FIG. 10. As in Fig. 8 for ^{94}Nb.

presented both graphically and in tabular form in Ref. 14.)

We should first look at Figs. 8—10 in low resolution. When this is done we see that the major discrepancies (see Fig. 5) between calculated (with the equidistant spacing model) and experimental spectra in the 0—4 MeV region of residual excitation are largely resolved. The large energy gap of nearly 4 MeV in ^{91}Zr (see also Fig. 4) is reproduced quite well, as is the decrease in gap in going to ^{92,94}Zr. The results in low resolution are in agreement with the qualitative predictions we made in Sec. III A and with the trend observable in the ^{90,91,92,94}Zr(p,n) data measured at 15° with 45 MeV protons.[29] These very large effects make one point fairly clear: Attempts to understand precompound spectra at low residual energies in terms of an equidistant model with a pairing correction are surely of questionable value for closed or near-closed-shell nuclei. The issue is more complicated and involves shell effects which are considerably more important than the pairing effects and which act in a very different manner with target neutron or proton number.

A more detailed comparison of calculated and experimental results in Figs. 8—10 shows a better agreement between calculated and experimental peak positions than might have been expected based on caveats stated earlier. The agreement is by no means quantitative. Some spectra are reproduced better with $(1p)(1n)^{-1}$ densities generated using single particle levels due to Seeger-Howard,[15] while others are better reproduced with levels due to Seeger-Perisho,[22] or are equally well reproduced by either set. The basis of what constitutes agreement is of course highly subjective. Clearly any structure in the experimental spectra due to collective states should not be reproduced in detail. Our calculation has the appropriate degrees of freedom to describe both the isobaric analog state (IAS) and Gamow-Teller (GT) transitions, but not to represent these peak structures in detail because of the lack of a two-body force and limitations caused by the choice of single particle energies. Specifically, if one uses single particle level energies which are completely isospin symmetric, the analog state will include the appropriate strength in one peak. It can also be located at the proper position if the Fermi energy differences are chosen appropriately. Our single particle level schemes were not completely isospin consistent, so this spreads the strength out somewhat. Similarly, if the single particle energies are chosen so that each charge exchange spin flip transition has the same energy, a giant GT state will be produced. Our single energies did not meet this criterion precisely and the experimental GT strength is not as concentrated in a narrow energy region as is the case for the analog. Thus for both the analog and the GT states, the strength will be correctly given but details of the energy dependence will be incorrect because of the lack of a two-body force.

We do see in these figures that results are strongly dependent on the locations of the single particle levels entering the calculations, which in turn also depend on the spreading due to deformation, including the sign of the deformation. This raises the exciting possibility that experimental precompound spectra could be used as a guide to setting centroids of excited single particle levels. This would mean that models and data heretofore associated with an understanding of smooth continuous spectra could become a tool of nuclear structure physics; it remains to be seen if this speculation is within bounds of reason.

It may be seen from these comparisons that precompound decay spectra may be expected to show peak structure at low residual excitations (for near-closed-shell nuclei) simply due to considerations of realistic single particle levels. Here it is worth mentioning that for the residual nuclei under consideration the density of resolved levels[30] exceeds 20 MeV^{-1} at 2 MeV of excitation. Yet the question is often asked of "precompound practitioners" as to how to remove the "smooth" precompound background from observed peak structure in an experimental measurement. From Figs. 8—10 it should be clear that the peaks may well *be* the precompound contribution; the only reason that calculated precompound spectra appear smooth at low excitations is that an equidistant single particle level assumption has been used in generating the exciton densities used as input to the calculations, forcing the resulting smooth spectral predictions.

It was shown in the early work on this subject by Williams *et al.*,[1] that as target nuclei become deformed the splitting of the degeneracy of single particle levels very quickly causes a disappearance of the shell effects under discussion; it was further demonstrated (by calculation[1,2]) that an equidistant spacing model should be a good approximation in such cases. In Fig. 11 we show a calculated $(1p)(1n)^{-1}$ state density for the residual nucleus of the ^{159}Tb(p,n)^{159}Dy reaction, the experimentally measured neutron spectrum, and the result of the geometry dependent hybrid (GDH) calculation using the equidistant spacing model. The $(1p)(1n)^{-1}$ exciton configuration densities were calculated with Seeger-Perisho single particle levels, an averaging width of 1.5 MeV, and pairing energies of 1.02 MeV. An experimentally deduced (for neighboring

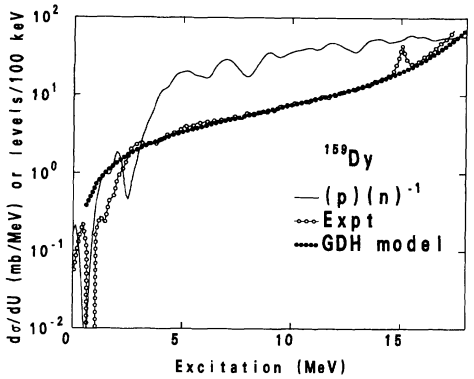

FIG. 11. Calculated and experimental results for ^{159}Tb(p,n). The solid curve is the $(1p)(1n)^{-1}$ two quasiparticle density for ^{159}Dy with $\delta=0.31$ plotted as levels per 100 keV. Open points joined by line segments are the experimental angle integrated spectrum for 25 MeV proton energy. The dashed curve is the result of the geometry dependent hybrid model (GDH). The GDH and experimental results are plotted as mb/MeV vs residual excitation.

nuclei) nuclear deformation parameter $\delta=0.31$ was used.[31] At this deformation the equidistant spacing model is a good approximation of the single particle level distribution, e.g., of Ref. 22, and the agreement of the experimental and calculated spectra confirms the earlier predictions of Ref. 2. For this case the GDH model with equidistant spacing model densities gives a spectrum without the deficiencies (or much less in magnitude) than those shown in Fig. 5.

V. CONCLUSIONS

We have shown that large gaps near the end points of precompound spectra may be observed for nuclei which are near-closed shells, with a generalization that an understanding of these gaps requires a consideration of relevant single particle orbitals, and not simply of a pairing term. We see that these effects are expected to "wash out" fairly rapidly with nuclear deformation. Simple considerations of shell model levels allow us to understand these effects in a qualitative manner.

More detailed comparisons may be made between experimental precompound spectra, and calculated $(1p)(1n)^{-1}$ state densities. We have made such comparisons. A list of effects was given which weaken the expected agreement between calculated and experimental results. Whether to characterize the comparisons as good or poor is subjective. We feel that the degree of agreement is very encouraging. A more rigorous treatment of angular momentum, and of locations of excited state single particle levels holds some promise of further improving this agreement, and therefore of performing more microscopic precompound calculations in the future. Ultimately we might better be able to identify spectral peaks resulting from simple excitation by a two-body operator versus those of a different nature. We believe that it is fair to say that even the relatively primitive microscopic particle-hole densities presented herein provide a much improved description of our experimental results than the equidistant spacing model.

It is possible that precompound spectra may ultimately be used to determine centroids of $(1p)(1n)^{-1}$ excited states, thereby becoming a tool of nuclear structure research. To do so will require first the inclusion of angular momentum in the quasiparticle state density calculations.

ACKNOWLEDGMENTS

One of the authors (MB) wishes to acknowledge helpful discussions with Prof. Peter Möller and Dr. George Leander. This work was performed under the auspices of the U.S. Department of Energy by the Lawrence Livermore National Laboratory under Contract Number W-7405-ENG-48. Two of the authors (W.S. and M.T.) acknowledge partial support by the Bundesministerium für Forschung und Technologie (BMFF).

---

*Permanent address: Department of Physics, Ohio University, Athens, OH 45701.

†Permanent address: I. Institut für Experimentalphysik, Zyklotron, Universität Hamburg, Hamburg, Federal Republic of Germany.

[1]F. C. Williams, Jr., A. Mignerey, and M. Blann, Nucl. Phys. **A207**, 619 (1973).

[2]K. Albrecht and M. Blann, Phys. Rev. C **8**, 1481 (1973).

[3]S. M. Grimes, J. D. Anderson, J. W. McClure, B. A. Pohl, and C. Wong, Phys. Rev. C **7**, 343 (1973); S. M. Grimes, J. D. Anderson, J. C. Davis, and C. Wong, *ibid.* **8**, 1770 (1973).

[4]S. M. Grimes, J. D. Anderson, and C. Wong, Phys. Rev. C **13**, 2224 (1976); C. Wong, J. D. Anderson, J. C. Davis, and S. M. Grimes, *ibid.* **7**, 1895 (1973).

[5]W. Scobel, L. F. Hansen, B. A. Pohl, C. Wong, and M. Blann, Z. Phys. A **311**, 323 (1983).

[6]C. Kalbach, S. M. Grimes, and C. Wong, Z. Phys. A **275**, 175 (1975).

[7]J. C. Davis, J. D. Anderson, E. K. Freytag, and D. R. Rawles, IEEE Trans. Nucl. Sci. **NS-20**, 213 (1973).

[8]C. Wong, S. M. Grimes, C. H. Poppe, V. R. Brown, and V. A. Madsen, Phys. Rev. C **26**, 889 (1982).

[9]B. D. Walker, J. D. Anderson, J. W. McClure, and C. Wong, Nucl. Instrum. Methods **29**, 333 (1964).

[10]R. C. Haight and D. R. Dalgas, Nucl. Instrum. Methods **165**, 55 (1979).

[11]C. F. Williamson, J. P. Boujot, and J. Picard, Saclay Report CEA-R3042, 1966.

[12]W. J. Courtney and J. D. Fox, At. Data Nucl. Data Tables **15**, 141 (1975).

[13]J. D. Anderson, C. Wong, and J. W. McClure, Phys. Rev. **138**, B615 (1965).

[14]W. Scobel *et al.*, Lawrence Livermore National Laboratory Report UCID-20101, 1984 (unpublished).

[15]P. A. Seeger and W. M. Howard, Nucl. Phys. **A238**, 491 (1975).

[16]C. Kalbach, Z. Phys. A **283**, 401 (1977).

[17]N. Rosenzweig, Phys. Rev. **105**, 950 (1957).

[18]M. Blann, Phys. Rev. Lett. **28**, 757 (1972).

[19]M. Blann and H. K. Vonach, Phys. Rev. C **28**, 1475 (1983).

[20]T. E. O. Ericson, Adv. Phys. **9**, 423 (1960).

[21]S. G. Nilsson, K. Dan. Vidensk. Selsk. Mat.-Fys. Medd. **29**, No. 16 (1955).

[22]P. A. Seeger and R. C. Perisho, Los Alamos National Laboratory Report No. LA3751, 1967 (unpublished).

[23]J. Bardeen, L. N. Cooper, and J. R. Schrieffer, Phys. Rev. **108**, 1175 (1957); L. G. Moretto, Nucl. Phys. **A182**, 641 (1972); S. M. Grimes, in *Theory and Application of Moment Methods in Many Fermion Systems,* edited by B. J. Dalton, S. M. Grimes, J. P. Vary, and S. A. Williams (Plenum, New York, 1979), p. 17.

[24]A. Gilbert and A. G. W. Cameron, Can. J. Phys. **43**, 1446 (1965).

[25]A. N. Behkami and J. R. Huizenga, Nucl. Phys. **A217**, 78 (1973).

[26]S. Åberg, Phys. Scr. **25**, 23 (1982).

[27]M. Blann, Phys. Rev. Lett. **27**, 337 (1971); **27**, 700(E) (1971); **27**, 1550(E) (1971).

[28]M. Blann and J. Bisplinghoff, Lawrence Livermore National Laboratory Report UCID-19614, 1982 (unpublished).

[29]W. A. Sterrenberg, S. M. Austin, U.E.P. Berg, R. de Vito, and A. I. Galonsky, Bull. Am. Phys. Soc. **24**, 649 (1979); A. I. Galonsky, in *The (p,n) Reaction and the Nucleon-Nucleon Force* (Plenum, New York, 1980), p. 191.

[30]*Table of Isotopes*, 7th ed., edited by C. M. Lederer and V. S. Shirley (Wiley, New York, 1978).

[31]P. H. Stelson and L. Grodzins, Nucl. Data Tables **A1**, 21 (1965).